A loaded Timoshenko beam bonded to an elastic half plane

L. Lanzoni [a,b,*], E. Radi [c]

[a] DIEF-Dipartimento di Ingegneria Enzo Ferrari, Università di Modena e Reggio Emilia, 41125 Modena, Italy
[b] DESD-Dipartimento di Economia, Scienze e Diritto, Università degli Studi di San Marino, 47890 San Marino Città Repubblica di San Marino
[c] DISMI-Dipartimento di Scienze e Metodi dell'Ingegneria, Università di Modena e Reggio Emilia, 42122 Reggio Emilia, Italy

ABSTRACT

The problem of a Timoshenko beam of finite length loaded by concentrated forces and couples and perfectly bonded to a homogeneous elastic and isotropic half plane is considered in the present work. In particular, the effects induced by shear deformation of the beam on the contact stresses arising at the interface between the beam and the underlying half plane are investigated accurately. An asymptotic analysis of the stress field at the beam ends and in the neighborhood of the loaded section of the beam allows us to characterize the singular nature of the peeling and shear stresses. The problem is formulated by imposing the strain compatibility condition between the beam and the half plane, thus leading to a system of two singular integral equations with Cauchy kernel. The unknown interfacial stresses are expanded in series of Jacobi orthogonal polynomials displaying complex singularity. This approach allows us to handle the oscillatory singularity and to reduce the integral equations to a linear algebraic system of infinite equations for the unknown coefficients of the interfacial stresses, which is solved through a method of collocation. The interfacial peeling and shear stresses and, in turn, the displacement field along the contact region have been calculated under various loading conditions applied to the beam. The internal forces and bending moments along the beam have been calculated varying the shear and flexural stiffness of the beam. The complex stress intensity factors and the strength of the stress singularities have been assessed in detail.

© 2016 Elsevier Ltd. All rights reserved.

1. Introduction

Contact problems between beams, plates, bars, strips etc. and an elastic substrate attracted a lot of interest in the field of solid mechanics in order to predict the mechanical behavior of a variety of composites systems, specially used in civil and mechanical engineering. As an example, steel panels and plates are often stiffened by metallic strip-like elements in order to increase their out-of-plane strength, their bending stiffness and, in turn, their buckling load. This is a key issue concerning offshore platforms, bridge decks and other kinds of structures which require high-performance mechanical behavior, avoiding excessive weight and materials consumption (e.g. Grondin et al., 1999).

Fibre reinforced polymer (FRP) bonding is widely used as an effective method to strengthen existing reinforced concrete (RC) elements, thus improving their resistance and toughness and, in turn, their service life. Typical failure mode affecting this kind of sys-

tems occurs with an interfacial crack between the FRP stiffener and the RC plate, growing toward the free ends of the stiffener (Oehlers and Seracino, 2004).

In the framework of civil engineering, simplified analyses of the soil-structure interaction are usually performed by modeling the building foundations like beams (for strip-like foundation) or plates (for raft foundation) supported by an elastic half plane (e.g. Wolf, 1988).

In the last decades, the scientific community has focused its attention in renewable energy generators. Among these, a promising technique to produce "green" energy consists in applying piezoelectric patch-like or strip-like transducers to existing flexible structures (typically, cantilever beams and walls), thus converting the vibration motion of the hosting structural elements into electrical energy. Similarly, smart sensors and actuators can be applied to existing structures to monitoring their mechanical behavior in time (e.g. Lin and Liu, 2006).

In microelectronics, many MEMS and NEMS like bulk acoustic resonators, high density capacitors, coplanar plate varactors, skin-like circuits, crystalline undulators (e.g. Guidi et al., 2007; Lanzoni et al., 2008; Lanzoni and Radi, 2009) and other miniaturized packages involve thin films and coatings deposited onto a substrate (Gevorgian, 2009; Shen, 2010). These microsystems are often

subjected to high residual stresses taking place during their fabrication process (a comprehensive reference about the mechanical behavior of piezoelectric multilayer actuators can be found in Ballas, 2007).

In order to predict the mechanical response of this kind of composite structures, a proper investigation of the stress and strain fields arising at the interface is mandatory. Special attention must be paid to stress and strain concentrations which can lead to loss of adhesion, debonding and other damaging phenomena affecting the durability and stability of this kind of devices.

In many studies, films (or stiffeners) bonded to a compliant substrate are modeled like bars or membranes, neglecting their bending stiffness. Such an assumption allows ignoring the interfacial peeling stress. As an example, Arutiunian (1968) solved the problem of a thin film bonded to an elastic half plane subjected to a thermal variation. Later, a simpler method was adopted by Erdogan and Gupta (1971) and Morar and Popov (1971), who solved the problem of a strip bonded to a half plane subjected to axial loads applied at the ends of the coating. Using a similar approach, Guler (2008) considered the problem of thin cover plates bonded to a graded substrate. A detailed analysis about the stress singularity in thin films welded to an elastic half plane under various loading conditions can be found in Lanzoni (2011) (for the stress singularities of a membrane stiffener with variable thickness see also Erdogan and Ozturk, 2008). A bar model has been adopted by Villaggio (2003) to study the brittle detachment of a stiffener welded to an elastic plate.

A number of numerical analyses have been also performed to study the mechanical behavior of single or multi-layered systems involving thin films and coatings. As an example, finite element–boundary integral equation methods (FE-BIE) have been widely used to investigate bars and membranes bonded to an elastic half plane (e.g. Takahashi and Shibuya, 1997, 2003; Tullini et al, 2012). In these studies, the problem is devised by using a mixed variational formulation involving the Green function for the half plane.

Nonetheless, if the coating flexural stiffness becomes significant, then the membrane models become inappropriate and the bending rigidity of the coating must be necessarily taken into account. In this case, both shear and peeling stresses arise at the interface between the cover and the substrate.

One of the earliest studies concerning the contact problem among beam elements has been performed by Timoshenko (1925). This author studied a bimetal strip under bending or thermal loads and solved the problem by imposing the compatibility between the axial strains of both beams in contact, neglecting the occurrence of interfacial stresses. Later, the approach has been extended by Suhir (1986) by introducing "interfacial compliance" parameters to describe the deformation of the cross section of the beams under the shearing load over the beam thickness. Moreover, the interfacial shear and peeling stresses are found as exponential functions of the axial coordinate. This method has been employed to investigate the effects induced by thermal stress in multilayered structures (Suhir, 1988) and the peeling stress as a function of a "through-thickness" spring parameter (Suhir, 1989). Indeed, the approach adopted by Timoshenko (1925) gives exact results only if the Young modulus multiplied by the square of the thickness for the two strips is the same (Moore and Jarvis, 2004).

Shield and Kim (1992) performed an analytical study dealing with an Euler-Bernoulli beam welded to an elastic half plane under symmetric loads applied at the ends of the beam. These Authors expanded the interfacial stresses in series of orthogonal Chebyshev polynomials displaying square root singularity at the beam ends. As pointed out by the Authors, the membrane approximation may provide rough predictions, in particular for systems sensitive to mode I failure.

However, the Euler–Bernoulli beam model cannot be adopted for analyzing elements characterized by a significant shear deformation, like short beams, or when the constituent material is compliant with respect to shear loads, like for FRP profiles, whose polymeric (thermoset or thermoplastic) matrix exhibits low shear strengths and shear moduli (Barbero, 1999). In such cases, the Timoshenko beam model reveals more effective than the Euler–Bernoulli theory, in particular for dynamical analyses. As an example, transversal vibrations of railways have been studied taking into account their cross-sectional deformation by modeling the railway track as Timoshenko beams on elastic ground (Wu et al., 1999). Moreover, Timoshenko beam theory has been recently used to investigate the vibration frequencies of carbon nanotubes characterized by small length-to-diameter ratios (e.g. Wang et al., 2006).

Only few analytical studies dealing with Timoshenko beams in contact with elastic substrates can be found in the Literature. Among these, Essenburg (1962) considered a Timoshenko beam supported by a Winkler foundation and he found a closed form solution of the governing equation. Li et al. (1988) studied the unilateral frictionless contact between a Timoshenko beam resting on an elastic layer supported by a rigid base by using a Gauss–Chebyshev quadrature method. Bjarnehed (1993) performed a numerical investigation of the problem of a Timoshenko beam resting on an elastic cushion bonded to an orthotropic half plane. Tezzon et al. (2015) used a coupled FE-BIE method to model shear deformable beams bonded to an isotropic elastic half-space. However, to the authors knowledge, a closed form solution of the interfacial stress field of a Timoshenko beam bounded to a half plane under various loading conditions has not been found yet.

In the present work, the contact problem of a Timoshenko beam of finite length bonded to a homogeneous elastic half plane is investigated. The proposed approach consists in the imposition of the strain compatibility condition between the beam and the half plane by expanding the interfacial stresses in series of orthogonal Jacobi polynomials. This representation allows to remove the singularity of the integral equations derived from the strain compatibility condition. Then, by using a collocation technique, the problem is reduced to a linear algebraic system of equations for the unknown coefficients of the series expansions for the interfacial stresses. The present study allows to investigate the distribution of peeling and shear interfacial stresses within the contact region varying the stiffness parameters of the beam, with particular emphasis to the effects of shear deformation. A detailed analysis of the strength of the stress singularities at the ends of the beam is provided. In this respect, the present study represents an extension of the work performed by Shield and Kim (1992).

The paper is organized as follows. In Section 2, the governing equations for the beam and the half plane are reported and the method used to solve the singular integral equations is discussed therein. An asymptotic analysis of the interfacial stresses at the beam ends is performed in Section 3.1. The singular nature of the interfacial stresses in the neighborhood of a concentrated load applied at the inner of the beam is investigated in Section 3.2. Some relevant loading conditions are discussed in detail in Section 4. The main results in terms of interfacial stresses distribution, stress intensity factors and strength of stress singularities are reported for some typical symmetric as well as skew-symmetric loading conditions in Section 5. Finally, conclusions are drawn in Section 6.

2. Governing equations

Let us consider a Timoshenko beam of length $2a$ with a rectangular cross section of height h and unitary width, subjected to a system of axial and shear forces (N_1, N_2), (T_1, T_2) and bending moments (M_1, M_2) applied at both ends of the beam (shear forces are taken positive if upward directed; axial forces are
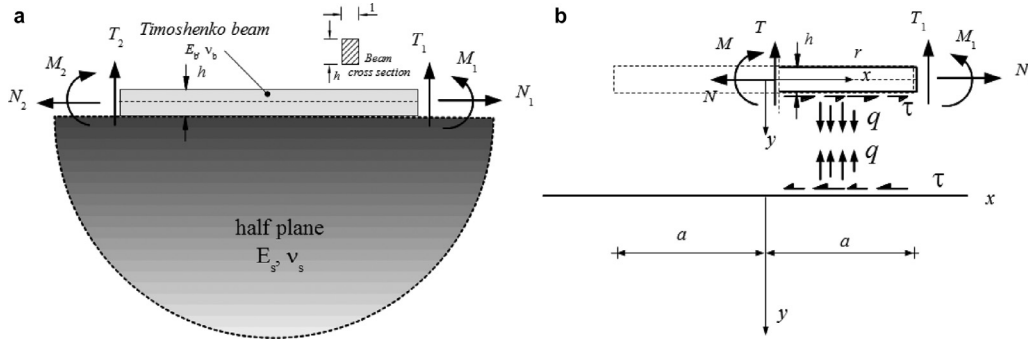
Fig. 1. A Timoshenko beam bonded to a half plane (a); free-body diagram of a beam bonded to a half-plane subjected to edge loads (b).

positive if rightward directed, bending moments are positive if counterclockwise), as shown in Fig. 1. The beam is supposed perfectly bonded to an elastic half plane. In absence of further external loads applied to the system, the equilibrium equations of the beam read:

$$N' + \tau = 0, \quad T' + q = 0, \quad M' - T + \tau\frac{h}{2} = 0, \tag{1}$$

being N, T and M the internal axial force, shear force and bending moment, respectively, applied at the beam cross section, whereas τ and q denote the shear and peeling tractions, respectively, (positive directions are depicted in Fig. 1b), arising at the interface between the beam and the half plane, and prime denotes differentiation with respect to coordinate x, namely $(\ldots)' = \partial(\ldots)/\partial x$.

The constitutive relations together with the kinematic assumptions for the Timoshenko beam give:

$$\frac{M}{E_b I} = \varphi', \quad u'_b = \frac{N}{E_b A} + \varphi'\frac{h}{2}, \quad v'_b = -\varphi + \frac{\chi T}{G_b A} \tag{2}$$

where $E_b = E_0$ or $E_0/(1-\nu_b^2)$ denote the Young modulus of the beam under generalized plane stress or plain strain conditions, respectively, ν_b is the Poisson ratio of the beam, A and I are the area and the moment of inertia of the beam cross section respectively, G_b represents the shear modulus of the beam, whereas χ denotes the dimensionless shear factor, i.e. $\chi = 6(1 - \nu_b\, G_b/E_b)/5$ or $\chi = [6 - \nu_b(1 + \nu_b)\, G_b/E_b]/5$ under plane stress or plane strain conditions, respectively (Cowper, 1966; Tullini et al., 2013). Note that, in Eq. (2), $\nu_b(x)$ denotes the transverse deflection of the beam along the y axis, $u_b(x)$ is the axial displacement of the beam cross section at the interface, i.e. at $y = 0$, and $\varphi(x)$ denotes the rotation of the beam cross section, positive if counterclockwise. According to the classical beam theory, the cross section of the beam is assumed to preserve its planarity after bending. The equilibrium conditions of the beam read:

$$N(x) = N_1 + \int_x^a \tau(s)\,ds, \quad T(x) = -T_1 + \int_x^a q(s)\,ds,$$

$$M(x) = M_1 + T_1(a - x) + \frac{h}{2}\int_x^a \tau(s)\,ds$$

$$+ \int_x^a q(s)(x - s)\,ds, \quad \text{for } |x| \le a. \tag{3}$$

Then, by assuming a unitary width of the beam cross section (i.e. $A = 1 \cdot h$), the axial strain along the interface reads:

$$u'_b(x) = \frac{N_1}{E_b h} + \frac{1}{E_b h}\int_x^a \tau(s)\,ds + \frac{h}{2E_b I}[M_1 + T_1(a - x)]$$

$$+ \frac{h}{4E_b I}\int_x^a [h\tau(s) + 2q(s)(x - s)]\,ds, \quad \text{for } |x| \le a. \tag{4}$$

The rotation $\varphi(x)$ of the beam cross section is found by integrating Eq. (2)$_1$:

$$\varphi(x) = \frac{M_1 x}{E_b I} + \frac{T_1}{2E_b I}(2ax - x^2) + \frac{h}{2E_b I}x\int_x^a \tau(s)\,ds$$

$$+ \frac{h}{2E_b I}\int_0^x s\tau(s)\,ds - \frac{1}{2E_b I}\int_0^a s^2 q(s)\,ds$$

$$+ \frac{1}{2E_b I}\int_x^a (s - x)^2 q(s)\,ds + \varphi_p, \quad \text{for } |x| \le a, \tag{5}$$

being φ_p a constant of integration to be determined. Thus, the slope $v'_b(x)$ of the beam reads:

$$v'_b(x) = -\frac{M_1 x}{E_b I} - \frac{T_1}{2E_b I}(2ax - x^2) - \frac{h}{2E_b I}x\int_x^a \tau(s)\,ds$$

$$- \frac{h}{2E_b I}\int_0^x s\tau(s)\,ds + \frac{1}{2E_b I}\int_0^a s^2 q(s)\,ds +$$

$$- \frac{1}{2E_b I}\int_x^a (s - x)^2 q(s)\,ds - \varphi_p - \frac{\chi T_1}{G_b h}$$

$$+ \frac{\chi}{G_b h}\int_x^a q(s)\,ds, \quad \text{for } |x| \le a, \tag{6}$$

where relation (2)$_3$ for the Timoshenko beam has been used. Note that the slope v'_b is positive if clockwise, according to the reference system adopted (see Fig. 1b).

The mechanical behavior of the homogeneous isotropic elastic half plane is defined by the Poisson ratio ν_s and the Young modulus, namely E_s under plane stress condition or $E_s/(1-\nu_s^2)$ under plane strain condition. Then, the normal strains at the boundary of the half plane become (Johnson, 1985):

$$u'_s(x) = -\frac{2}{E_s\pi}\int_{-a}^a \frac{\tau(\xi)}{\xi - x}d\xi + \left(\frac{2}{E_s} - \frac{1}{2G_s}\right)q(x)$$

$$v'_s(x) = -\frac{2}{E_s\pi}\int_{-a}^a \frac{q(\xi)}{\xi - x}d\xi - \left(\frac{2}{E_s} - \frac{1}{2G_s}\right)\tau(x), \quad \text{for } |x| \le a, \tag{7}$$

being $G_s = E_s/2(1 + \nu_s)$ the shear modulus of the half plane.

The strain compatibility conditions between the beam and the half plane require:

$$u'_b(x) = u'_s(x), v'_b(x) = v'_s(x), \quad \text{for } |x| \le a. \tag{8}$$

After the introduction of (7), eqns (8) form a system of two singular integral equations with Cauchy kernel, which can be straightforwardly solved following Erdogan et al. (1973) by expanding the unknown shear and peeling stresses in series of Jacobi orthogonal

polynomials, namely:

$$\tau(x) = E_s(a+x)^s(a-x)^s \sum_{n=0}^{\infty} C_n P_n^{(s,s)}(x/a),$$

$$q(x) = E_s(a+x)^s(a-x)^s \sum_{n=0}^{\infty} D_n P_n^{(s,s)}(x/a), \quad \text{for } |x| \leq a, \quad (9)$$

where $P_n^{(s,s)}(x)$ is the Jacobi polynomial of order n and the index s of the polynomials denotes the singular strength of the interfacial stresses at the end of the bonded region, i.e. at $x = \pm a$, where $\text{Re}(s) = -1/2$ will be found in Section 3,. Therefore, series expansions (9) allow to remove the singularity in Eq. (8), being $(a+x)^s (a-x)^s$ the proper weight function for $P_n^{(s,s)}(x)$ (see Appendix A). By introducing the representation (9) for the interfacial stresses, the singular integrals involved in Eqs. (7) and (8) can be evaluated in closed form by using the results (A4)-(A5). Hence, if a finite number N of terms is considered in the series (9), then the compatibility conditions (8) are imposed in $N+1$ properly selected collocation points x_k. As well known, in the present case, the optimal collocation points are the roots of the Jacobi polynomial $P_{N+1}^{(s,s)}(x)$, i.e. $x_k : P_{N+1}^{(s,s)}(x_k) = 0$, with $k = 1, 2, ..., N+1$. Since an explicit closed form expression for the roots x_k of the Jacobi polynomials cannot be found, then the roots of the real Jacobi polynomial $P_{N+1}^{(-1/2,-1/2)}(x)$ have been chosen here as collocation points for the sake of simplicity, namely

$$x_k = \cos\left(\frac{\pi k}{2(N+1)}\right), \text{ with } k = 1, 2, ..., N+1, \quad (10)$$

coinciding with the roots of the Chebyshev polynomial of first kind of order $N+1$. The proposed approach allows us to transform the integro-differential system (8) into a linear algebraic system that can be solved for the unknown coefficients C_n, D_n of the interfacial stresses introduced in (9) up to an arbitrary large value of terms. The regularity of this kind of algebraic system and the rate of convergence have been studied in detail (e.g. Erdogan, 1969).

Once the strain field at the interface is known, the displacement field of the beam at the interface can be obtained by properly integrating the strain field of the beam:

$$u_b(x) = -\frac{N_1 x}{E_b A} + \frac{h}{4E_b I}[2M_1 x + T_1(2ax - x^2)] + \left(\frac{1}{E_b A} + \frac{h^2}{4E_b I}\right)$$

$$\times \left[x \int_x^a \tau(s)ds + \int_0^x s\tau(s)ds\right]$$

$$+ \frac{h}{4E_b I}\left[\int_x^a q(s)(x-s)^2 ds - \int_0^a s^2 q(s)ds\right] + u_p, \quad \text{for } |x| \leq a,$$

$$v_b(x) = -\frac{M_1 x^2}{2E_b I} - \frac{T_1}{6E_b I}(3ax^2 - x^3) - \frac{h}{2E_b I}\left[\frac{x^2}{2}\int_x^a \tau(s)ds\right.$$

$$\left. + \frac{1}{2}\int_0^x s^2\tau(s)ds\right]$$

$$- \frac{h}{2E_b I}\left[\int_0^a s(x-s)\tau(s)ds\right] + \frac{x}{2E_b I}\int_0^a s^2 q(s)ds - \frac{1}{2E_b I}$$

$$\times \left[\int_x^a q(s)(xs^2 + \frac{x^3}{3} - x^2 s)ds + \frac{1}{3}\int_x^a q(s)ds\right] +$$

$$- \varphi_p x - \frac{\chi T_1}{G_b A}x + \frac{\chi}{G_b A}\left[x \int_x^a q(s)ds + \int_0^x sq(s)ds\right]$$

$$+ v_p, \quad \text{for } |x| \leq a, \quad (11)$$

being u_p and v_p constant of integrations of the displacement field which assessment is not mandatory as they represent arbitrary rigid motions.

Furthermore, by integrating equations (7), the displacements of the points on half plane surface read (Johnson, 1985):

$$u_s(x) = \frac{2}{E_s \pi}\int_{-a}^a \tau(\xi)\text{Log}|\xi - x|d\xi + \left(\frac{1}{E_s} - \frac{1}{4G_s}\right)$$

$$\times \left[\int_{-a}^x q(\xi)d\xi - \int_x^a q(\xi)d\xi\right],$$

$$v_s(x) = \frac{2}{E_s \pi}\int_{-a}^a q(\xi)\text{Log}|\xi - x|d\xi - \left(\frac{1}{E_s} - \frac{1}{4G_s}\right)$$

$$\times \left[\int_{-a}^x \tau(\xi)d\xi - \int_x^a \tau(\xi)d\xi\right] \quad (12)$$

Note that the frictionless contact can be simply retrieved by solving Eq. (8)$_2$ for $\tau(x) = 0$. On the other hand, the purely membrane behavior of the coatings can be recovered by considering Eq. (8)$_1$ only, neglecting the terms depending upon the bending rigidity $E_b I$. Moreover, the behavior of an Euler–Bernoulli beam can be exactly retrieved by solving the system (8) neglecting the terms depending upon the shear stiffness G_b/χ (namely for $G_b/\chi \to \infty$). Also the (frictionless or not) contact problem of a rigid indenter applied at the surface of a half plane is provided by the present approach for large values for the parameter $E_b I$.

Note that the problem is governed by three independent dimensionless parameters, namely E_s/E_b, a/h and $E_s \chi /G_b$. The first parameter accounts for the relative stiffness of the beam with respect that of the half plane; whereas the second one depends on the slenderness of the beam. The shear stiffness of the beam is taken into account through the third parameter: as it increases, the shear compliance of the beam increases with respect its flexural compliance, thus increasing the effects induced by shear deformation on the system.

It is worth noting that all the integrals involved in the expressions (7), (11), (12) and, in turn, the displacements and the internal forces applied to the beam can be calculated in closed form by means of the relations reported in Appendix.

3. Asymptotic analysis

3.1. Asymptotic analysis of the interfacial stresses at the beam ends

In the present section, the behavior of the stress and displacement fields at the beam ends is investigated by performing a preliminary asymptotic analysis by imposing the continuity of tractions and displacement between the beam and the elastic half plane (a comprehensive review about the origins of asymptotic procedures in stress analysis can be found in Hills et al. (2004)). From Eqs. (1) to (2), the following differential equations hold for the Timoshenko beam:

$$E_b A\left(u_b'' - \varphi''\frac{h}{2}\right) + \tau = 0, \quad \frac{G_b A}{\chi}(v_b'' + \varphi') + q = 0,$$

$$E_b I\varphi''' + q + \tau'\frac{h}{2} = 0. \quad (13)$$

Then, by using relations (13), the interfacial stresses can be expressed in terms of the displacement field as:

$$\tau = -E_b A\left(u_b'' - \varphi''\frac{h}{2}\right), \quad q = -E_b I\varphi''' + E_b A\frac{h}{2}\left(u_b'''' - \varphi'''\frac{h}{2}\right) = 0. \quad (14)$$

With reference to a polar coordinate system $\{r, \theta\}$ centered at the left end of the beam (see Fig. 2a), an Airy stress function for the asymptotic fields in the isotropic half plane near the end points of the beam can be assumed in the form $\phi(r, \theta) = \text{Re}[r^{s+2} F(\theta)]$, where the complex exponent s defines the stress singularity and
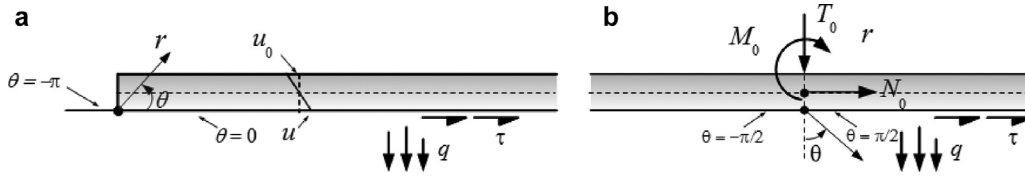
Fig. 2. Polar coordinate system adopted for the asymptotic analysis at the beam edges (a) and at an inner loaded section (b).

the function:

$$F(\theta) = a \sin(s+2)\theta + b \cos(s+2)\theta + c \sin s\theta + d \cos s\theta, \qquad (15)$$

provides the angular variation of the asymptotic fields (Williams, 1959). The corresponding stress components in the isotropic half space near the left end of the beam are:

$$\sigma_{\theta\theta} = \frac{\partial^2 \phi}{\partial r^2} = \text{Re}[r^s(s+1)(s+2)F(\theta)],$$

$$\sigma_{r\theta} = -\frac{\partial}{\partial r}\left(\frac{\partial \phi}{r\partial\theta}\right) = -\text{Re}[r^s(s+1)F'(\theta)]. \qquad (16)$$

Due to the continuity of tractions across the interface, a similar asymptotic behavior must be imposed for the interfacial stresses at the beam ends, i.e.:

$$\tau = \text{O}(r^s), \quad q = \text{O}(r^s), \quad \text{as } r \to 0. \qquad (17)$$

Then, in order to accomplish relations (13)–(14) as r approaches 0, the displacement and rotation fields of the beam must display the following asymptotic behavior:

$$\varphi = \text{O}(r^{s+2}), \quad u = \text{O}(r^{s+2}), \quad v = \text{O}(r^{s+2}), \quad \text{as } r \to 0. \qquad (18)$$

The displacement field within the half plane corresponding to the Airy stress function (16) (see Barber (2010), Tables 8.I and 9.I) under plane strain condition reads (Williams, 1959):

$$u_\theta = \frac{1}{2G_s}r^{s+1}[-F'(\theta) - 4(1-\nu_s)(c\cos s\theta - d\sin s\theta)] + \text{O}(r^{s+2}),$$

$$u_r = \frac{1}{2G_s}r^{s+1}[-(s+2)F(\theta) + 4(1-\nu_s)(c\sin s\theta + d\cos s\theta)]$$
$$+ \text{O}(r^{s+2}), \text{ as } r \to 0. \qquad (19)$$

Therefore, the Airy stress function must satisfy the following conditions in order to match with the asymptotic behavior of the displacement of the beam along the interface (18), namely at $\theta = 0$:

$$F'(0) + 4c(1-\nu_s) = 0, \quad (s+2)F(0) - 4d(1-\nu_s) = 0. \qquad (20)$$

Namely, at leading order the constraint due to the beam on the elastic half plane is equivalent to a rigid constraint. Moreover, the boundary conditions on the free boundary of the half plane, i.e. at $\theta = -\pi$, require:

$$\sigma_{\theta\theta}(-\pi) = r^s(s+1)(s+2)F(-\pi) = (b+d)\cos\pi s$$
$$-(a+c)\sin\pi s = 0,$$
$$\tau(-\pi) = r^s(s+1)F'(-\pi) = [cs + a(s+2)]\cos\pi s$$
$$+[b(s+2)+ds]\sin\pi s = 0. \qquad (21)$$

Conditions (20) and (21) lead to an algebraic homogeneous linear system that can be written in the following matrix form:

$$\begin{pmatrix} 2+s & 0 & 4+s-4\nu_s & 0 \\ 0 & 2+s & 0 & s-2+4\nu_s \\ -\sin\pi s & \cos\pi s & -\sin\pi s & \cos\pi s \\ (2+s)\cos\pi s & (2+s)\sin\pi s & s\cos\pi s & s\sin\pi s \end{pmatrix}$$

$$\times \begin{pmatrix} a \\ b \\ c \\ d \end{pmatrix} = \begin{pmatrix} 0 \\ 0 \\ 0 \\ 0 \end{pmatrix}. \qquad (22)$$

The system (22) admits non trivial solution if and only if the following characteristic equation holds true:

$$e^{4\pi i s} + 2\frac{5 - 4\nu_s(3 - 2\nu_s)}{3 - 4\nu_s}e^{2\pi i s} + 1 = 0. \qquad (23)$$

Eq. (23) admits the roots $e^{2\pi i s} = -(3-4\nu_s)^{\pm 1}$. Then, in order to recover a finite energy flux as r approaches 0, the admissible stress singularity obtained from Eq. (23) is

$$s = -\frac{1}{2} + i\varepsilon, \quad \text{where} \quad \varepsilon = \frac{1}{2\pi}\ln(3 - 4\nu_s), \qquad (24)$$

as well as its conjugate value $\bar{s}$. Therefore, the real part of the exponent s is $-1/2$ whatever be the Poisson ration ν_s of the substrate. As expected, the imaginary part of s depends on the Poisson ratio of the half plane ν_s only. Note that Eq. (20) of Shield and Kim (1992) is exactly retrieved. Note also that the classical square root singularity, namely $s = -1/2$, is recovered for $\nu_s = 0.5$ (incompressible half plane).

The angular variation of the Airy stress function (15) corresponding to the eigenvalue (24) provided by the eigenvalue problem (22) is then

$$F(\theta) = 2Ce^{-\frac{3}{2}i\theta}e^{\varepsilon\theta}\{(1+2i\varepsilon)e^{2i\theta}\sin\theta + i[e^{i\theta} + e^{2\varepsilon(\pi+\theta)}]\}, \qquad (25)$$

where C is a real constant that cannot be determined from the eigenvalue problem (22). Note that the eigenfunction corresponding to the eigenvalue $\bar{s}$ is just the complex conjugate of $F(\theta)$, so that

$$\phi(r,\theta) = Cr^{\frac{3}{2}}\text{Re}[r^{i\varepsilon}F(\theta)]. \qquad (26)$$

The stress field corresponding to the Airy stress function (26) is then

$$\sigma_{\theta\theta} = Cr^{-\frac{1}{2}}\text{Re}\left[\left(\frac{1}{2}+i\varepsilon\right)\left(\frac{3}{2}+i\varepsilon\right)r^{i\varepsilon}F(\theta)\right],$$

$$\sigma_{r\theta} = -Cr^{-\frac{1}{2}}\text{Re}\left[\left(\frac{1}{2}+i\varepsilon\right)r^{i\varepsilon}F'(\theta)\right]. \qquad (27)$$

According to Rice (1988), the complex stress intensity factor $K = K_1 + i K_2$ can be defined as the limit

$$K = \sqrt{2\pi}\lim_{r\to 0}\frac{(\sigma_{\theta\theta} + i\sigma_{r\theta})_{\theta=0}}{r^{-\frac{1}{2}+i\varepsilon}}$$

$$= C\sqrt{\frac{\pi}{2}}(1 + e^{2\pi\varepsilon})[-8\varepsilon + (3 - 4\varepsilon^2)i]. \qquad (28)$$

A similar analysis can be performed also under plane stress condition. In this case the oscillatory singularity is defined by the coefficient

$$\varepsilon = \frac{1}{2\pi} \ln \frac{3 - v_s}{1 + v_s}. \tag{29}$$

3.2. Asymptotic analysis of the interfacial stresses at the loaded section

The behavior of the stress field in the neighborhood of a concentrated load applied at the middlespan of a Timoshenko beam is investigated in the present section. In this case, the slope of the Timoshenko beam displays a discontinuity at the point of application of a transversal load due to the shear deformability of the beam. As a consequence, by considering a power law singularity as in Section 3.1 no solution can be found which satisfies the continuity of tractions and displacements between the beam and the half plane. Therefore, we have to look for a more general asymptotic expansion of the stress and displacement fields in the half plane under the loaded section, which allows for a logarithmic stress singularity as suggested by Sinclair (2004).

Making reference to a polar coordinate system $\{r, \theta\}$ centered at the middlespan of the beam (see Fig. 2b) in correspondence of the loaded section, the leading order stress and displacement fields in the elastic half plane take the following form according to Sinclair (2004):

$$\sigma_{\theta\theta}(r,\theta) = (1 + \ln r)[c_1 \cos 2\theta + c_2 \sin 2\theta] + (3 + 2\ln r)c_3$$
$$- \theta(c_1 \sin 2\theta - c_2 \cos 2\theta - 2c_4),$$
$$\sigma_{r\theta}(r,\theta) = (1 + \ln r)[c_1 \sin 2\theta - c_2 \cos 2\theta] + \theta(c_1 \cos 2\theta$$
$$+ c_2 \sin 2\theta) - c_4,$$
$$u_r(r,\theta) = \frac{r}{2G_s}\{(c_1 \cos 2\theta + c_2 \sin 2\theta)\ln r + [1 + (1-\kappa)\ln r]c_3$$
$$- \theta(c_1 \sin 2\theta - c_2 \cos 2\theta) +$$
$$- (1-\kappa)c_4\},$$
$$u_\theta(r,\theta) = \frac{r}{2G_s}\{(c_1 \sin 2\theta - c_2 \cos 2\theta)\ln r - [1 + (1+\kappa)\ln r]c_4$$
$$+ \theta(c_1 \cos 2\theta + c_2 \sin 2\theta)$$
$$+ (1+\kappa)c_3\}, \tag{30}$$

being $\kappa = 3 - 4v_s$ for plane strain and $\kappa = (3-v_s)/(1+v_s)$ for plane stress.

By assuming a logarithmic singularity for the interfacial stress field under the loaded section of the beam, i.e.:

$$\tau = O(\ln r), \quad q = O(\ln r), \quad \text{as } r \to 0, \tag{31}$$

then, the coefficient multiplied by $r \ln r$ in the displacement components $(30)_{3,4}$ must vanish. It follows that the displacement field of the elastic half plane must satisfy the following two independent conditions:

$$c_1 + (\kappa - 1)c_3 = 0, \quad c_2 - (\kappa + 1)c_4 = 0, \tag{32}$$

Accordingly, the asymptotic behavior of the interfacial stresses become:

$$\sigma_{\theta\theta}(r,\pi/2) = c_3[2 + \kappa + (1+\kappa)\ln r] + c_4\pi(1-\kappa)/2,$$
$$\sigma_{\theta\theta}(r,-\pi/2) = c_3[2 + \kappa + (1+\kappa)\ln r] + c_4\pi(\kappa-1)/2,$$
$$\sigma_{r\theta}(r,\pi/2) = c_4[\kappa + (1+\kappa)\ln r] + c_3\pi(\kappa-1)/2,$$
$$\sigma_{r\theta}(r,-\pi/2) = c_4[\kappa + (1+\kappa)\ln r] + c_3\pi(1-\kappa)/2, \text{ as } r \to 0. \tag{33}$$

It is worth noting that the axial strain and the slope of the beam are discontinuous at $x = 0$, namely across the section of the beam where the external loads and moment are applied. Indeed, the presence of the axial load N_0, the transverse load T_0 and the couple M_0 applied at the section $x = 0$ yield therein a jump in the axial strain $u_b'(0)$, in the slope $v_b'(0)$ and in the curvature of the beam at $x = 0$, respectively:

$$[u_b'(0)] = \frac{N_0}{E_b A}, \quad [v_b'(0)] = -\frac{\chi T_0}{G_b A}, \quad [u_b'(0)] = -\frac{M_0 h}{2E_b I}, \tag{34}$$

where $[f(x)]$ denotes the jump of the function $f(x)$ at x. Obviously, discontinuities in the stress field of the half plane also occur in light of the strain compatibility conditions (8), and these conditions allow to find out the constants c_3, c_4.

In particular, if a concentrated axial load N_0 acts at the middlespan of the beam, then, due to symmetry, one has $\tau(x) = \tau(-x)$ and $q(x) = -q(-x)$, so that $c_3 = 0$ and the peeling stress turns out to be discontinuous across the section at $x = 0$, namely:

$$\tau(x) \sim c_4[\kappa + (1+\kappa)\ln|x|], \quad q(x) \sim c_4\pi(\kappa-1)\text{sign}(x)/2. \tag{35}$$

Furthermore, by imposing that $[u_s'(0)] = N_0/E_b A$, and inserting expressions (35) into the expression of the axial strain of the half plane surface $(7)_1$, one finds:

$$c_4 = \frac{E_s}{2\pi} \frac{N_0}{E_b A} \frac{1}{(1+v_s)\kappa}. \tag{36}$$

The case of a couple M_0 applied at the middlespan of the beam is analogous to that of a concentrated axial load. In this case, according to $(34)_3$, one has $[u_s'(0)] = M_0 h/2E_b I$, $c_3 = 0$ and

$$c_4 = \frac{E_s}{4\pi} \frac{M_0 h}{E_b I} \frac{1}{(1+v_s)\kappa}. \tag{37}$$

Note that, the slope $v_s'(x)$ under a concentrated axial load or couple, is continuous across the loaded section, namely at $x = 0$. Note also that, for an Eulero–Bernoulli beam loaded by a concentrated axial load or couple, the same asymptotic behavior (35) is found for the interfacial stresses.

A transversal concentrated load applied at the middlespan of the beam produces a jump in the slope of the beam according to $(34)_2$, so that $[v_s'(0)] = -\chi T_0/G_b A$. Symmetry conditions imply $\tau(x) = -\tau(-x)$ and $q(x) = q(-x)$, so that $c_4 = 0$. Then, the interfacial stresses in the neighborhood of the loaded section of the beam behave asymptotically as:

$$\tau(x) \sim c_3\pi(\kappa-1)\text{sign}(x)/2, \quad q(x) \sim c_3[2+\kappa + (1+\kappa)\ln|x|], \tag{38}$$

where

$$c_3 = \frac{E_s}{2\pi} \frac{\chi T_0}{G_b A} \frac{1}{(1+v_s)\kappa}. \tag{39}$$

Differently from the problem of an E–B beam loaded by a concentrated axial load or couple, the axial strain $u_s'(x)$ is continuous across the section loaded by the transversal load. In this case, both the strain and stress fields of the beam and, in turn, those of the elastic half plane are continuous across the loaded section of the beam (see Appendix B).

4. Results related to some relevant loading cases

4.1. Solution of symmetric edge-loading condition

In this section, a symmetric loading applied at the beam ends is considered (see Fig. 3a). Owing to symmetry, both integration constants φ_p and u_p are zero. Moreover, the interfacial shear stress τ is
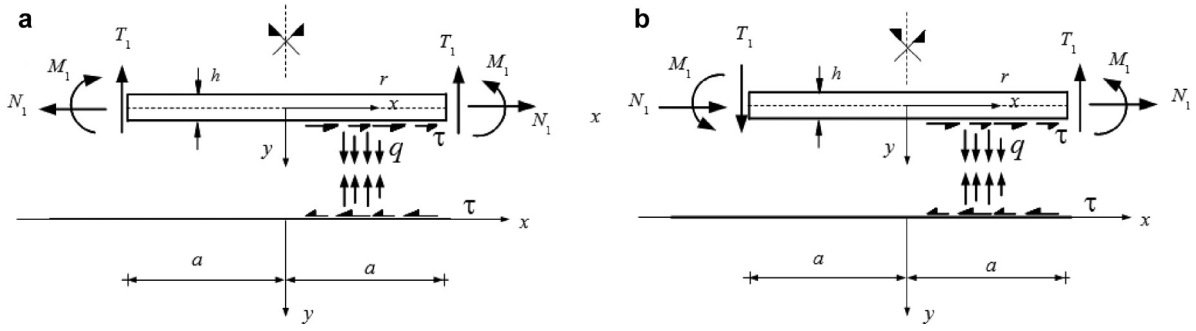
Fig. 3. Beam/half-plane system subjected to symmetric (a) and skew-symmetric (b) edge loads.

an odd function, whereas the peeling stress q is an even function. Thus, the interfacial shear and peeling stresses can be straightforwardly expanded in series of Jacobi polynomials, namely:

$$\tau(x) = E_s(a+x)^s(a-x)^s \sum_{n=1,3,}^{2N+1} C_n P_n^{(s,s)}(x/a),$$

$$q(x) = E_s(a+x)^s(a-x)^s \sum_{n=0,2,4,}^{2N} D_n P_n^{(s,s)}(x/a), \quad \text{for } |x| \leq a, \quad (40)$$

being $P_n^{(s,s)}$ the Jacobi polynomials of order n.

The equilibrium conditions of the beam along the x and y axes require

$$\int_{-a}^{a} \tau(s)ds = 0, \quad \int_{-a}^{a} q(s)ds = 2T_1, \quad (41)$$

respectively. Note that condition $(41)_1$ is fulfilled since expression $(40)_1$ does not contain the term C_0. Moreover, the equilibrium condition $(41)_2$ entails (see identity A3):

$$D_0 = \frac{2T_1 \Gamma(3/2+s)}{a^{2s+1} E_s \sqrt{\pi} \Gamma(s+1)}. \quad (42)$$

Actually, being D_0 given by Eq. (42), condition $(8)_1$ is imposed at the $N+1$ collocation points, whereas condition $(8)_2$ is imposed at the same points except x_{N+1}. Thus, the system of 2 integral equations (8) leads to an algebraic system of $2N+1$ equations in the $N+1$ unknowns coefficients C_i ($i = 1, 3, 5, ..., 2N+1$), and N coefficients D_j ($j = 2, 4, ..., 2N$).

The singular behavior of the interfacial stresses at the beam ends ($x = \pm a$) can be properly investigated by means of the peeling and shear stress intensity factors (SIFs) K_I and K_{II}, defined as (Mahajan et al., 2003):

$$K_I(\pm a) = \lim_{x \to \pm a} \frac{q(x)}{(a \mp x)^s} = \pm 2^s E_s a^s \sum_{n=0,2,}^{N} D_n P_n^{(s,s)}(\pm 1),$$

$$K_{II}(\pm a) = \lim_{x \to \pm a} \frac{\tau(x)}{(a \mp x)^s} = \pm 2^s E_s a^s \sum_{n=1,3}^{N} C_n P_n^{(s,s)}(\pm 1), \quad (43)$$

respectively.

4.2. Solution of skew-symmetric edge-loading condition

In this section, a skew-symmetric loading condition is considered, as shown in Fig. 3b. Similarly to the symmetric layout, now the interfacial shear stress τ must be an even function, whereas the peeling stress q is an odd function. The integration constant φ_p is a further unknown to be determined by solving the strain compatibility condition, whereas v_p is null. Thus, the interfacial shear and peeling stresses can be expanded in series of Jacobi polynomi-
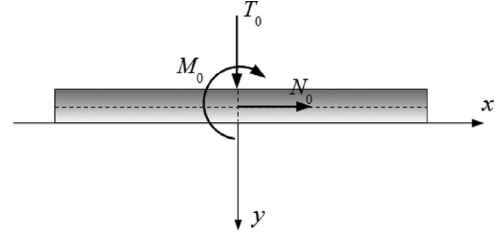

Fig. 4. Timoshenko beam bonded to a half-plane subjected to concentrated loads.

als as follows:

$$\tau(x) = E_s(a+x)^s(a-x)^s \sum_{n=0,2,4,}^{2N} C_n P_n^{(s,s)}(x/a),$$

$$q(x) = E_s(a+x)^s(a-x)^s \sum_{n=1,3,}^{2N+1} D_n P_n^{(s,s)}(x/a), \quad \text{for } |x| \leq a. \quad (44)$$

The equilibrium conditions of the beam along the x and y axes require

$$\int_{-a}^{a} \tau(s)ds = 2N_1, \quad \int_{-a}^{a} q(s)ds = 0. \quad (45)$$

Note that condition $(28)_2$ is fulfilled since expression $(27)_2$ does not contain the term D_0; moreover, the equilibrium condition $(28)_1$ entails:

$$C_0 = \frac{2N_1 \Gamma(3/2+s)}{a^{2s+1} E_s \sqrt{\pi} \Gamma(s+1)}. \quad (46)$$

The strain compatibility conditions (8) are imposed at the $N+1$ collocation points x_k given in Eq. (10). Here, both conditions (8) are imposed at the $N+1$ collocation points, thus giving an algebraic system of $2(N+1)$ equations in the N unknowns coefficients C_i ($i = 2, 4, 6, ..., 2N$), $N+1$ coefficients D_j ($j = 1, 3, ..., 2N+1$) and the unknown φ_p.

4.3. Solution of concentrated loads applied at the middlespan of the beam

Let consider a Timoshenko beam bonded to a half plane and subjected to a concentrated axial load N_0 or a couple M_0 applied at the middlespan section, as reported in Fig. 4. In this case, the interfacial stresses are assumed in the form:

$$\tau(x) = E_s(a+x)^s(a-x)^s \sum_{n=0,2,4,}^{2N} C_n P_n^{(s,s)}(x/a) + c_4(1+\kappa)\ln|x/a|,$$

$$q(x) = E_s(a+x)^s(a-x)^s \sum_{n=1,3,}^{2N+1} D_n P_n^{(s,s)}(x/a)$$

$$+ c_4 \frac{\pi}{2}(\kappa-1)\text{sign}(x), \quad \text{for } |x| \leq a, \quad (47)$$
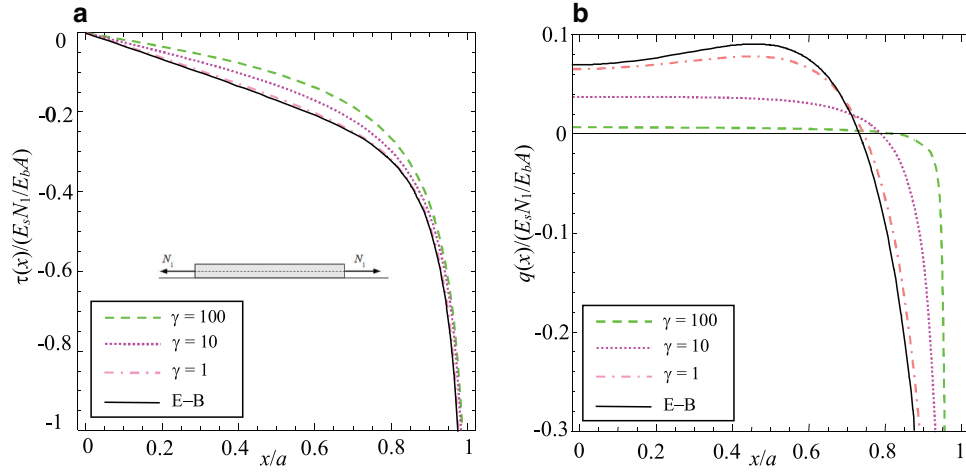
Fig. 5. Beam subject to two horizontal end forces: dimensionless (a) interfacial shear stress and (b) peeling stress for $\gamma = 100$ (green dashed line), $\gamma = 10$ (magenta dotted line), $\gamma = 1$ (pink dash-dot line) and for an Euler-Bernoulli beam (black solid line). Symmetry holds for negative x coordinate.

where the constant c_4 is given by (36) or (37) according to the loading condition.

If a concentrated transversal load T_0 acts at the middlespan of the beam (see Fig. 4a), the following expressions are considered for the interfacial stresses:

$$\tau(x) = E_s(a+x)^s(a-x)^s \sum_{n=1,3,}^{2N+1} C_n P_n^{(s,s)}(x/a) + c_3 \frac{\pi}{2}(1-\kappa)\text{sign}(x),$$

$$q(x) = E_s(a+x)^s(a-x)^s \sum_{n=0,2,4,}^{2N} D_n P_n^{(s,s)}(x/a)$$
$$+ c_3(1+\kappa)\ln|x/a|, \quad \text{for } |x| \le a, \quad (48)$$

where the constant c_3 takes the expression (39).

5. Results

Results in terms of interfacial shear and peeling tractions are given in the present section varying the dimensionless parameter $\gamma = E_s \chi / G_b$. Note that small values of the parameter γ denote a beam with high shear rigidity; conversely, large values of γ denote compliant beams with respect the substrate in terms of shear deformation. The case of an Euler–Bernoulli beam can be recovered as the limiting case of a Timoshenko beam for $\gamma \to 0$. All the results reported in the following have been obtained by assuming plane stress condition and, for sake of definiteness, $\nu_b = 0$; $\nu_s = 0.2$, $E_s/E_b = 0.1$ and $a/h = 5$. Symmetric edge loading conditions are considered first.

The dimensionless shear and peeling stresses $\tau(x)/(N_1/E_bA)$, $q(x)/(N_1/E_bA)$ of a Timoshenko beam loaded at its ends by two symmetric axial loads N_1 are reported in Fig. 5 versus the dimensionless longitudinal coordinate x/a, for different values of the parameter γ, namely $\gamma = 1, 10, 100$ (label "E–B" in the plot legend stands for Euler–Bernoulli beam). As reported in Fig. 5a, as γ increases, the interfacial shear stress monotonically decreases (in modulus) within the whole contact region, and the maximum magnitude of the stress distribution occurs for $\gamma = 0$, i.e. for an Euler-Bernoulli beam. Conversely, the peeling stress exhibits a non-monotonic trend within the contact region, as reported in Fig. 5b. In particular, it is compressive in the neighborhoods of the beam ends, whereas it becomes tensile under the middle part of the beam. Indeed, the tensile end forces N_1 together with the interfacial shear tractions deflect the beam and tend to uplift it from

the half plane in the middle of the contact region. As expected, for large values of γ the peeling stress tends to concentrate at the beam ends; conversely, as γ decreases, it becomes significant also at the middlespan of the beam. Note that the effect of a thermal variation ΔT acting on the beam can be recovered by applying two opposite axial end loads $N_1 = E_b A \alpha_b \Delta T$, being α_b the coefficient of thermal expansion of the beam.

A beam loaded by two transversal loads applied at its ends has been also considered (see Fig. 6). Differently from the previous loading case, the peeling stress exhibits monotonic behavior within the whole contact region, whereas the interfacial shear stress displays opposite signs at the middlespan and at the ends of the beam. Moreover, the shear tractions change sign and quickly grow up at the beam ends, thus exhibiting a boundary layer behavior accordingly to the results obtained by Shield and Kim (1992) for the Euler–Bernoulli beam. In particular, the zero of the shear stress is found to move toward the beam ends increasing γ, and the magnitude of the shear tractions increases with γ in proximity of the beam ends. This trend is confirmed by the analysis of the SIFs also (see Fig. 11b).

The interfacial tractions due to two opposite end couples are shown in Fig. 7. For such a loading condition, the variation of the peeling stress along the interface displays a trend similar to that observed for a beam subjected to two axial loads applied at the beam ends. Conversely, the magnitude of the interfacial shear tractions grows up near the beam ends as γ increases. However, a non-monotonic trend is observed in the middlespan of the beam varying γ, as reported in Fig. 7a. As expected, due to symmetry the shear stress vanishes at the middlespan of the beam whatever the parameter γ.

The shear and peeling stresses for a Timoshenko beam loaded by an internal axial load applied at the middlespan section are reported in Fig. 8a and b, respectively, for some specific values of the parameter γ. The shear stress is found to be almost independent of γ in the whole contact region. Moreover, as displayed by Fig. 8a, the shear stress is singular both at the ends ($x/a = \pm1$) and under the concentrated load (i.e. at $x = 0$), and it assumes the same sign within the whole contact region. As displayed in Fig. 8b, the peeling stress assumes finite values and vanishes at about 7/10 of the half-length of the beam whatever the parameter γ. Then, it takes the opposite sign going toward the beam ends, where it displays singular behavior. Note also that, according to expressions $(35)_2$ and (36), the jump exhibited by the peeling stress across
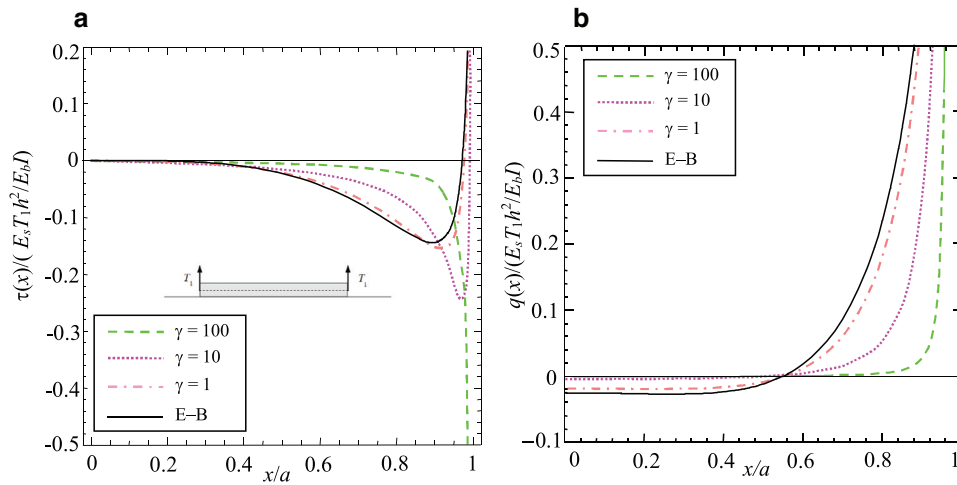
Fig. 6. Beam subject to two vertical end forces: dimensionless (a) interfacial shear stress and (b) peeling stress for $\gamma = 100$ (green dashed line), $\gamma = 10$ (magenta dotted line), $\gamma = 1$ (pink dash-dot line) and for an Euler-Bernoulli beam (black solid line). Symmetry holds for negative x coordinate.
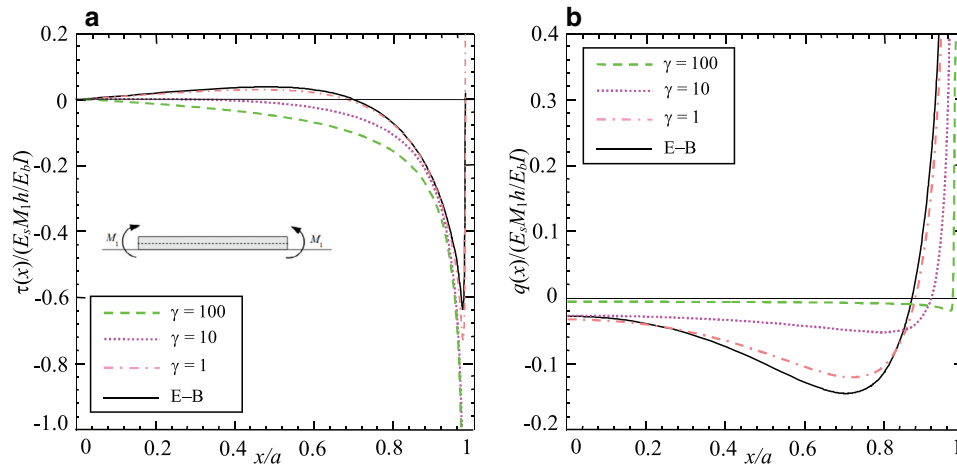

Fig. 7. Beam subject to two end moments: dimensionless (a) interfacial shear stress and (b) peeling stress for $\gamma = 100$ (green dashed line), $\gamma = 10$ (magenta dotted line), $\gamma = 1$ (pink dash-dot line) and for an Euler–Bernoulli beam (black solid line). Symmetry holds for negative x coordinate.
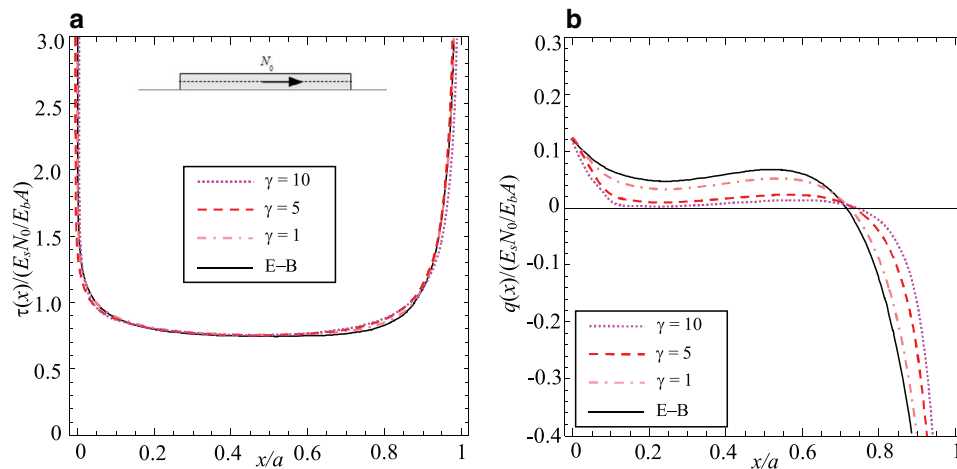

Fig. 8. Beam subject to a horizontal concentrated force a) interfacial shear stress and (b) peeling stress for $\gamma = 10$ (magenta dotted line), $\gamma = 5$ (red dashed line), $\gamma = 1$ (pink dash-dot line) and for an Euler–Bernoulli beam (black solid line). Symmetry holds for negative x coordinate.
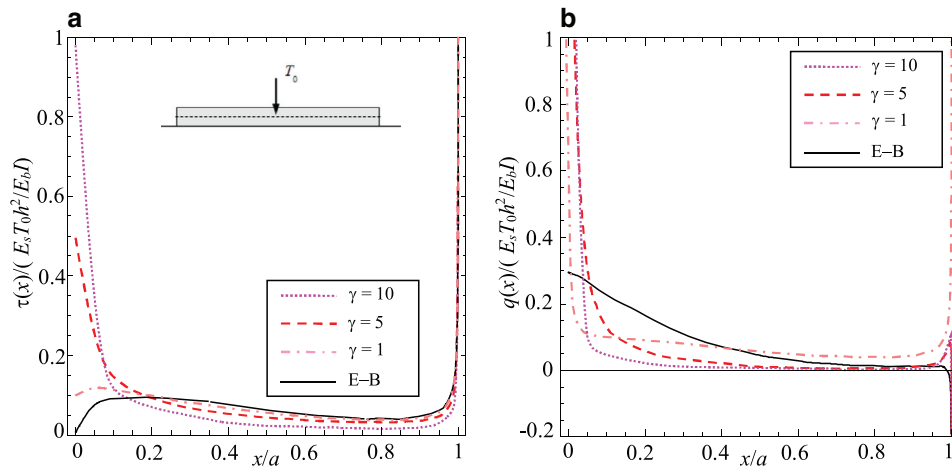
Fig. 9. Beam subject to a vertical concentrated force (a) interfacial shear stress and (b) peeling stress for $\gamma = 10$ (magenta dotted line), $\gamma = 5$ (red dashed line), $\gamma = 1$ (pink dash-dot line) and for an Euler-Bernoulli beam (black solid line). Symmetry holds for negative x coordinate.

Fig. 10. Beam subject to a couple (a) interfacial shear stress and (b) peeling stress for $\gamma = 10$ (magenta dotted line), $\gamma = 5$ (red dashed line), $\gamma = 1$ (pink dash-dot line) and for an Euler–Bernoulli beam (black solid line). Symmetry holds for negative x coordinate.
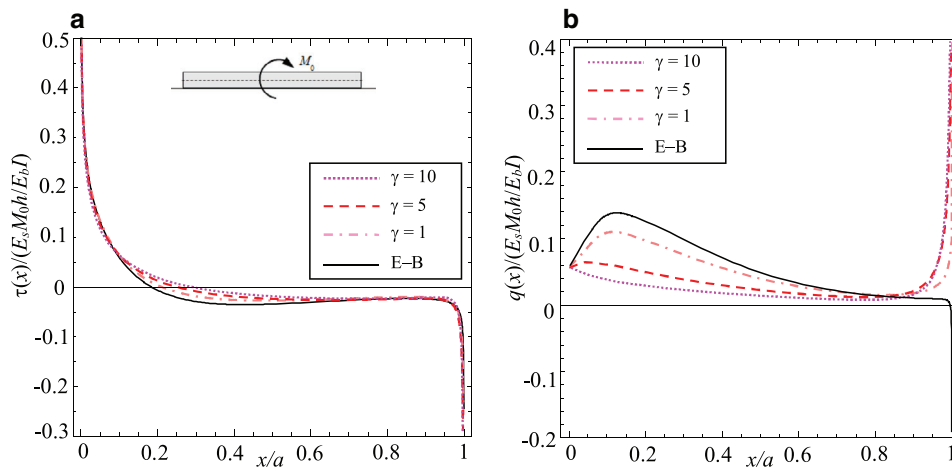
the loaded section does not vary with γ. In particular, for the values of the parameters here considered one finds $q(0)/(E_sN_0/E_bA) \cong 0.12518$.

The shear and peeling stresses under a beam loaded by a transversal concentrated force T_0 applied at the middlespan of the beam are reported in Fig. 9. Differently from the previous loading condition, the peeling stress is singular both at the middlespan of the beam and at the beam ends, whereas the shear stress is discontinuous across the loaded section, namely at $x = 0$. In particular, for $\gamma = 1, 5, 10$ one finds $\tau(0)/(E_sT_0h^2/E_bI) = 0.09921$; 0.49603; 0.99206, respectively, whereas $\tau(0) = 0$ for an Euler–Bernoulli beam. It is worth noting that both the shear and peeling stresses near the beam ends decrease as γ increases, whereas opposite behavior is observed in the neighborhood of the loaded section.

Fig. 10a and b concern the shear and peeling stresses of a Timoshenko beam loaded by a couple applied at the middlespan. As found for an axial concentrated load, the peeling stress is finite at $x = 0$, and one finds $q(0)/(E_sM_0h/E_bI) \cong 0.05952$ whatever the parameter γ. The largest values of the peeling stress along the bonded region occur for an Euler–Bernoulli beam. The shear stress is singular both at the beam ends and at the section loaded by the couple, and it does not significantly vary with γ. Differently

Table 1

Dimensionless real and imaginary parts of the stress intensity factors $K_I(a)$ and $K_{II}(a)$ for a beam subjected to symmetric and skew-symmetric horizontal forces at the ends.

Symmetric	E–B	$\gamma = 100$	$\gamma = 200$	$\gamma = 300$	$\gamma = 400$	$\gamma = 500$
Re(K_I)	0.240	0.008	0.006	0.004	0.004	0.003
Im(K_I)	0.624	0.081	0.056	0.043	0.035	0.029
Re(K_{II})	−1.365	−1.104	−1.079	−1.070	−1.064	−1.061
Im(K_{II})	−2.742	−2.245	−2.198	−2.179	−2.170	−2.164
Skew	E–B	$\gamma = 100$	$\gamma = 200$	$\gamma = 300$	$\gamma = 400$	$\gamma = 500$
Re(K_I)	0.569	−6.457	−8.254	−9.128	−9.646	−9.990
Im(K_I)	1.676	−12.861	−16.008	−17.813	−18.896	−19.618
Re(K_{II})	−5.104	−5.869	−5.722	−5.622	−5.555	−5.507
Im(K_{II})	−10.295	−12.918	−12.879	−12.862	−12.840	−12.821

from the case of an axial concentrated load, the shear stress at the beam ends assumes opposite sign with respect to that assumed in the neighborhood of the loaded section (from the same side).

Finally, the strength of the interfacial stresses has been studied for various loading conditions varying γ, as reported in Fig. 11. For convenience, the values of the stress concentration factors have been listed in Tables 1–6 for relevant values of the parameter γ for the examined loading cases. A remarkable difference between the
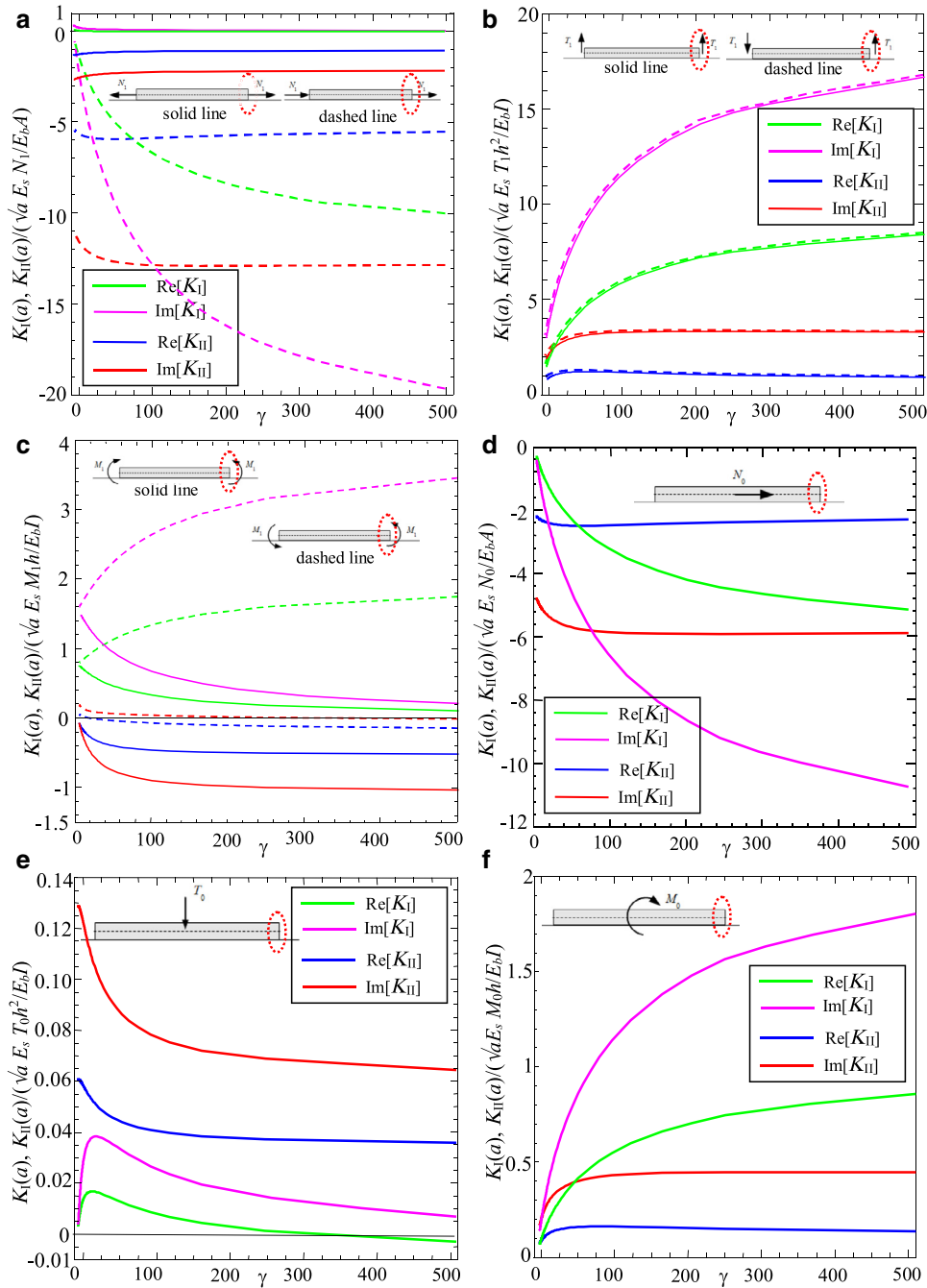
Fig. 11. Dimensionless real and imaginary parts of the stress intensity factors $K_I(a)$ and $K_{II}(a)$ for (a) horizontal end forces; (b) vertical end forces and (c) end couples; (d) horizontal midpoint force; (e) vertical midpoint force; (f) midpoint couple varying γ.

symmetric and skew-symmetric axial loads applied at the beam ends is displayed in Fig. 11a (see also Table 1). In particular, both the real and imaginary parts of the SIFs $K_I(a)$ and $K_{II}(a)$ are not significantly affected by the parameter γ when two opposite axial loads act on the beam ends. As expected, $K_{II}(a)$ is greater than $K_I(a)$. Conversely, when the axial loads have the same direction, then $K_{II}(a)$ is greater than $K_I(a)$ only for small values of the parameter γ. Indeed, both the real and imaginary parts of $K_I(a)$ monotonically increases with γ and they overcome those of $K_{II}(a)$ approximately for $\gamma > 90$. Fig. 11b and Table 2 deal with a Timoshenko beam loaded by two symmetric and skew-symmetric transversal end loads. No significant differences are found between these loading conditions. Indeed, for both loading conditions, the real and

Table 2
Dimensionless real and imaginary parts of the stress intensity factors $K_I(a)$ and $K_{II}(a)$ for a beam subjected to symmetric and skew-symmetric vertical forces at the ends.

Symmetric	E–B	$\gamma = 100$	$\gamma = 200$	$\gamma = 300$	$\gamma = 400$	$\gamma = 500$
$Re(K_I)$	0.818	5.852	7.181	7.829	8.213	8.468
$Im(K_I)$	1.598	11.442	14.081	15.390	16.176	16.700
$Re(K_{II})$	0.627	1.244	1.137	1.065	1.016	0.982
$Im(K_{II})$	1.354	3.332	3.388	3.382	3.370	3.359
Skew	E–B	$\gamma = 100$	$\gamma = 200$	$\gamma = 300$	$\gamma = 400$	$\gamma = 500$
$Re(K_I)$	0.826	5.893	7.212	7.854	8.236	8.488
$Im(K_I)$	1.611	11.523	14.149	15.450	16.230	16.751
$Re(K_{II})$	0.660	1.257	1.140	1.062	1.011	0.975
$Im(K_{II})$	1.422	3.355	3.388	3.371	3.352	3.336

Table 3
Dimensionless real and imaginary parts of the stress intensity factors $K_I(a)$ and $K_{II}(a)$ for a beam subjected to symmetric and skew-symmetric couples at the ends.

Symmetric	E–B	$\gamma = 100$	$\gamma = 200$	$\gamma = 300$	$\gamma = 400$	$\gamma = 500$
$Re(K_I)$	0.767	0.355	0.208	0.154	0.122	0.101
$Im(K_I)$	1.544	0.667	0.431	0.319	0.254	0.211
$Re(K_{II})$	0.085	−0.462	−0.496	−0.507	−0.512	−0.515
$Im(K_{II})$	0.249	−0.896	−0.979	−1.009	−1.024	−1.033
Skew	E–B	$\gamma = 100$	$\gamma = 200$	$\gamma = 300$	$\gamma = 400$	$\gamma = 500$
$Re(K_I)$	0.761	1.342	1.545	1.647	1.707	1.747
$Im(K_I)$	1.527	2.645	3.047	3.250	3.373	3.456
$Re(K_{II})$	0.133	−0.068	−0.104	−0.123	−0.134	−0.142
$Im(K_{II})$	0.345	0.043	0.018	0.004	−0.005	−0.012

Table 4
Dimensionless real and imaginary parts of the stress intensity factors $K_I(a)$ and $K_{II}(a)$ for a beam subjected to a horizontal midpoint force.

	E–B	$\gamma = 100$	$\gamma = 200$	$\gamma = 300$	$\gamma = 400$	$\gamma = 500$
$Re(K_I)$	0.194	−3.210	−4.215	−4.644	−4.873	−5.198
$Im(K_I)$	0.686	−6.748	−8.614	−9.614	−10.224	−10.736
$Re(K_{II})$	−1.999	−2.410	−2.397	−2.306	−2.269	−2.241
$Im(K_{II})$	−4.321	−5.969	−5.979	−5.941	−5.905	−5.900

Table 5
Dimensionless real and imaginary parts of the stress intensity factors $K_I(a)$ and $K_{II}(a)$ for a beam subjected to a vertical midpoint force.

	E–B	$\gamma = 100$	$\gamma = 200$	$\gamma = 300$	$\gamma = 400$	$\gamma = 500$
$Re(K_I)$	0.008	0.009	0.007	0.002	−0.001	−0.002
$Im(K_I)$	0.002	0.026	0.017	0.013	0.010	0.007
$Re(K_{II})$	0.061	0.040	0.036	0.033	0.033	0.032
$Im(K_{II})$	0.131	0.077	0.069	0.067	0.065	0.064

Table 6
Dimensionless real and imaginary parts of the stress intensity factors $K_I(a)$ and $K_{II}(a)$ for a beam subjected to a midpoint couple.

	E–B	$\gamma = 100$	$\gamma = 200$	$\gamma = 300$	$\gamma = 400$	$\gamma = 500$
$Re(K_I)$	−0.006	0.560	0.703	0.782	0.813	0.869
$Im(K_I)$	−0.014	1.154	1.497	1.618	1.712	1.801
$Re(K_{II})$	0.019	0.157	0.148	0.141	0.136	0.132
$Im(K_{II})$	0.038	0.415	0.405	0.406	0.406	0.405

crease with γ and they reach a plateau approximately for $\gamma > 100$. This trend is confirmed by the values reported in Table 6.

The effect of the slenderness a/h of the beam has not been discussed here because the parameter a/h plays a role similar to the parameter γ used by Lanzoni (2011) to investigate the contact problem of a thin film. Therefore, as the ratio a/h decreases, the interfacial stresses tend to concentrate at the beam ends and, accordingly, the stress intensity factors $K_I(\pm a)$ and $K_{II}(\pm a)$ are expected to increase (in modulus). This occurrence is confirmed also by the analysis performed by Shield and Kim (1992) for the problem of an Euler-Bernoulli beam bonded to an elastic half plane.

6. Conclusions

An analytical investigation of the interfacial stress field taking place in a Timoshenko beam bonded to an elastic half plane and subjected to various loading conditions has been performed in the present work. The problem has been solved by imposing the compatibility between the strain fields of the beam and the half plane, under plane strain or generalized plane stress conditions. The unknown interfacial stresses have been expanded in series of orthogonal Jacobi polynomials. The present study allows to evaluate in detail the influence of the shear deformation of the beam, together with its axial and bending stiffness, on the stress singularities and stress concentration factors produced by the action of concentrated external loads and couples. The asymptotic analysis of the stress field at the beam ends as well as in the neighborhood of concentrated loads applied at the middlespan of the beam has been carried out in order to properly assess the singular nature of the shear and peeling stresses. In particular, a complex power singularity of the interfacial stresses is found at the beam ends. The corresponding singularity oscillatory index is found to depend on the Poisson ratio of the half plane only. Moreover, under the action of a concentrated axial force or a couple applied at an inner section of the Timoshenko beam, a logarithmic singularity is found for the shear stress, whereas the peeling traction exhibits a finite jump across the loaded section of the beam, and a similar behavior is found also for an Euler–Bernoulli beam. In proximity of the inner section of a Timoshenko beam loaded by a concentrated transversal load, the peeling stress displays a logarithmic singularity whereas the shear stress is finite and discontinuous across the loaded section. If the same loading condition is applied to an E–B beam, then finite and continuous stress and strain fields are found. It is worth noting that the magnitude of the interfacial stresses in the neighborhoods of the loaded section can be found by imposing that the beam and the half plane suffer the same jump in the strain.

The present model can be straightforwardly used to properly investigate strain and stress concentrations in various composite systems, like microelectronic packages characterized by small length-to-thickness ratio, thick coating-substrates systems, short strip-like foundations, etc., where the effect induced by the shear deformation is expected to play a relevant role.

In a forthcoming work the Authors will perform the buckling analysis of a Timoshenko beam bonded to an elastic half plane under several loading conditions, thus evaluating the effect induced by the shear deformation on the critical buckling load and the corresponding deformed shapes of the beam.

imaginary parts of $K_I(a)$ monotonically increases with γ, whereas $K_{II}(a)$ is not significantly affected by variations of γ except for γ approaching 0.

The strength of the stress field for a beam loaded by end couples is reported in Fig. 11c. When the couples have the same sign, $K_I(a)$ monotonically decreases whereas $K_{II}(a)$ monotonically increases (in modulus) with γ. Conversely, when the couples have opposite signs, $K_I(a)$ monotonically increases whereas $K_{II}(a)$ is not significantly influenced by variation of γ, except for very small values of γ, as confirmed by Table 3.

The singularity of the interfacial stresses under a beam loaded by an inner axial concentrated load has been studied also, and relevant results are reported in Fig. 11d and Table 4. Similarly to the problem of two symmetric end couples, in this case also a monotonic trend is observed both for $K_I(a)$ and $K_{II}(a)$ varying γ. However, for sufficiently large values of γ, both the real and imaginary parts of $K_{II}(a)$ are not significantly influenced by the parameter γ. This behavior resembles that reported in Fig. 11a for two skew-symmetric axial loads.

A nonmonotonic trend of $K_I(a)$ with γ is observed in Fig. 11e for a beam subjected to a transversal load applied at the middlespan. In particular, both the real and imaginary parts of $K_I(a)$ attain a maximum approximately for $\gamma = 12$. Both the real and imaginary parts of $K_{II}(a)$ decrease instead with γ, and for $\gamma > 200$ the real part of $K_{II}(a)$ is almost constant (see also Table 5).

The singularity of the interfacial stresses when a couple acts at the middlespan of the beam is similar to that found for an inner axial concentrated load (see Fig. 11 d). As displayed in Fig. 11f, as γ increases both the real and imaginary parts of $K_I(a)$ and $K_{II}(a)$ in-

Acknowledgments

Appendix

A. Useful formulas and results

Some formulas and results that have been used in the main text are reported in the following.

The following identity based on the rule of integration by parts has been used to find the analytical expressions of the displacements and internal forces applied to the beam:

$$\int_0^\rho \dots \left(\int_0^\psi \left(\int_0^x (x-s)p(s)ds \right) dx \right) d\psi = \frac{1}{n!} \int_0^\rho (\rho-s)^n p(s)ds, \tag{A1}$$

where n is the number of integrations and $p(s)$ a given smooth function within the domains of integration.

As known, Jacobi polynomials $P_n^{(s,s)}(x)$ are orthogonal on the interval $[-1, 1]$ with respect the weight $(1+x)^s(1-x)^s$, i.e. (Szegö, 1939; Gradshteyn and Ryzhik, 2007):

$$\int_{-1}^1 (1+x)^s(1-x)^s P_n^{(s,s)}(x)P_m^{(s,s)}(x)dx$$
$$= \frac{2^{2s+1}\Gamma^2(s+n+1)}{n!(2s+1+2n)\Gamma(2s+1+n)}\delta_{nm}, \tag{A2}$$

with $Re(s) > -1$, and $m, n \in \mathbb{N}_0$.

From (A2), the following identity is retrieved, being $P_0^{(s,s)}(x) = 1$:

$$\int_{-1}^1 (1+x)^s(1-x)^s P_n^{(s,s)}(x)dx = \frac{2^{2s+1}\Gamma^2(s+1)}{\Gamma(2s+2)}\delta_{n0} = \frac{\sqrt{\pi}\Gamma(s+1)}{\Gamma(s+3/2)}\delta_{n0}, \tag{A3}$$

from which the Eulerian beta integral is obtained. Moreover, the following result holds:

$$\int_{-1}^1 x(1+x)^s(1-x)^s P_n^{(s,s)}(x)dx = \frac{\sqrt{\pi}\Gamma(s+2)}{2\Gamma(s+5/2)}\delta_{n1}. \tag{A4}$$

From the interfacial stresses (9b), the normal strains of the half plane can be calculated analytically by using the following result (e.g. Karpenko, 1966):

$$\int_{-1}^1 \frac{(1+x)^s(1-x)^s P_n^{(s,s)}(x)}{t-x}dx$$
$$= \pi \left[\cot(\pi s)P_n^{(s,s)}(t)(1+t)^s(1-t)^s - \frac{2^{2s}}{\sin(\pi s)}P_{n+2s}^{(-s,-s)}(t) \right]. \tag{A5}$$

The Jacobi polynomial can be represented in terms of the Gauss hypergeometric function $_2F_1(\dots)$ as (Abramowitz and Stegun, 1972):

$$P_n^{(s,s)}(t) = P_n^{(s,s)}(1)_2F_1\left(-n, 1+2s+n, 1+s, \frac{1-t}{2}\right). \tag{A6}$$

The displacements for the half plane surface can be evaluated in closed form by using the following identities based on relations (A5) and (A6):

$$\int_{-1}^1 Log|t-x|P_n^{(s,s)}(x)(1+x)^s(1-x)^s dx$$

$$= \begin{cases} \dfrac{\pi}{2n}\left(\cot[\pi(s+1)]P_{n-1}^{(s+1,s+1)}(t)(1+t)^{s+1}(1-t)^{s+1} \right. \\ \qquad \left. -\dfrac{2^{2(s+1)}}{\sin[\pi(s+1)]}P_{n+1+2s}^{(-s-1,-s-1)}(t) \right), \quad \text{for } n=1,2,3,\dots; \\[8pt] \dfrac{1}{2\Gamma(1/2+s)\Gamma(3/2+s)}\{2\pi\csc(\pi s)\Gamma(3/2+s)(-t\cos(\pi s)\Gamma \\ (1/2+s)_2F_1(1/2, -2s, 3/2, t^2) \\ +\sqrt{\pi}[_pF_q(\{1, -2s, 1, \{1-s, 2\}, 1/2\})+ \\ +(t-1)_pF_q(\{1, -2s, 1\}, \{1-s, 2\}, (1-t)/2)]) - 4^{-s}\pi\Gamma \\ (1+2s)(H_{1/2+s} + \ln(4))\}, \quad \text{for } n=0, \end{cases} \tag{A7}$$

being H_n the nth harmonic number and $_pF_q(\dots)$ is the regularized generalized hypergeometric function. Moreover, one has:

$$\int_{-1}^t (1+x)^s(1-x)^s P_n^{(s,s)}(x)dx - \int_t^1 (1+x)^s(1-x)^s P_n^{(s,s)}(x)dx$$
$$= \begin{cases} 2t_2F_1\left(\frac{1}{2}, -s, \frac{3}{2}, t^2\right), & \text{for } n=0; \\[6pt] -\dfrac{(1-t^2)^{s+1}}{n}P_{n-1}^{(s+1,s+1)}(t), & \text{for } n=1,2,3,\dots. \end{cases} \tag{A8}$$

In order to evaluate the internal forces and bending moment of the beam according to eqns (3), the following identities have been used

$$\int_t^1 (1+x)^s(1-x)^s P_n^{(s,s)}(x)dx$$
$$= \begin{cases} \dfrac{\sqrt{\pi}\Gamma(1+s)}{2\Gamma(3/2+s)} - t_2F_1\left(\frac{1}{2}, -s, \frac{3}{2}, t^2\right) & \text{for } n=0; \\[8pt] \dfrac{1}{2n}P_{n-1}^{(s+1,s+1)}(t)(1+t)^{s+1}(1-t)^{s+1} & \text{for } n=1,2,3,\dots; \end{cases}$$

$$\int_{-1}^t (1+x)^s(1-x)^s P_n^{(s,s)}(x)dx$$
$$= \begin{cases} \dfrac{\sqrt{\pi}\Gamma(1+s)}{2\Gamma(3/2+s)} + t_2F_1\left(\frac{1}{2}, -s, \frac{3}{2}, t^2\right) & \text{for } n=0; \\[8pt] \dfrac{1}{2n}\left[\left(\dfrac{1-(-1)^{n+1}}{2}\right)P_{n-1}^{(s+1,s+1)}(0) - P_{n-1}^{(s+1,s+1)}(t)(1+t)^{s+1} \right. \\ \left. (1-t)^{s+1} \right] & \text{for } n=1,2,3,\dots; \end{cases} \tag{A9}$$

being $|t| \leq 1$.

The stress intensity factors can be straightforwardly evaluated by considering that

$$P_n^{(s,s)}(1) = \frac{\Gamma(n+s+1)}{n!\Gamma(s+1)},$$
$$P_n^{(s,s)}(-1) = (-1)^n \frac{\Gamma(n+s+1)}{n!\Gamma(s+1)}. \tag{A10}$$

Moreover the following identities have been used to perform the asymptotic analysis reported in Section 3.2 (Boros and Moll, 2004):

$$\int_{-1}^{1} \frac{\ln|x|}{t-x} dx$$
$$= \left[\text{PolyLog}\left(2, \frac{1}{|t|}\right) - \text{PolyLog}\left(2, -\frac{1}{|t|}\right) - i\pi \ln|t| \right] \text{sign}(t),$$

$$\int_{-1}^{1} \frac{\text{sign}(x)}{t-x} dx$$
$$= \ln\left(\frac{1}{t^2} - 1\right), \quad \text{with } |t| \le 1. \tag{A11}$$

B. Asymptotic analysis of the interfacial stresses in the neighborhood of a transversal load applied to an Euler–Bernoulli beam

Let us consider an Euler–Bernoulli beam laying on an isotropic half plane and loaded by a transversal concentrated load T_0. By assuming that the normal and shear contact stresses under the loaded section behave as

$$\tau = O(x\ln|x|), \quad q = O(1), \quad \text{as } x \to 0 \tag{B1}$$

the general expression of the biharmonic Airy stress function for the isotropic half plane is given by the following series expansion (Sinclair, 2004):

$$\phi(r,\theta) = \sum_{n=0}^{\infty} r^{n+2} \{ c_{1n} \cos(n+2)\theta + c_{2n} \cos n\theta$$
$$+ [a_{1n} \cos(n+2)\theta + a_{2n} \cos n\theta] \ln r +$$
$$- \theta [a_{1n} \sin(n+2)\theta + a_{2n} \sin n\theta], \quad \text{as } r \to 0. \tag{B2}$$

Due to the symmetry of the problem here considered, only even terms in the angular coordinate θ have been retained in (B2). The corresponding stress components can be derived from the Airy stress function as

$$\sigma_{\theta\theta} = \frac{\partial^2 \phi}{\partial r^2}, \quad \sigma_{rr} = \frac{1}{r}\frac{\partial \phi}{\partial r} + \frac{1}{r^2}\frac{\partial^2 \phi}{\partial \theta^2}, \quad \sigma_{r\theta} = -\frac{\partial}{\partial r}\left(\frac{1}{r}\frac{\partial \phi}{\partial \theta}\right). \tag{B3}$$

Then, the following expressions for the stress field in the half plane are found from (B2) and (B3):

$$\sigma_{rr}(r,\theta)$$
$$= \sum_{n=0}^{\infty} r^n \{ [(1-2n)a_{2n} - (n+1)(n-2)c_{2n}]\cos n\theta$$
$$- [(3+2n)a_{1n} + (n+1)(n-2)c_{1n}]\cos(n+2)\theta$$
$$+ (n+1)[(2-n)a_{2n}\cos n\theta - (n+2)a_{1n}\cos(n+2)\theta]\ln r,$$
$$+ (n+1)[(2+n)a_{1n}\theta\sin(n+2)\theta + (n-2)a_{2n}\theta\sin n\theta]\},$$

$$\sigma_{\theta\theta}(r,\theta) = \sum_{n=0}^{\infty} r^n \{ [(3+2n)a_{1n} + (n+1)(n+2)c_{1n}]\cos(n+2)\theta$$
$$+ [(3+2n)a_{2n} + (n+1)(n-2)c_{2n}]\cos n\theta$$
$$+ (n+1)(n+2)[a_{1n}\cos(n+2)\theta + a_{2n}\cos n\theta]\ln r$$
$$- (n+1)(n+2)\theta[a_{1n}\sin(n+2)\theta - a_{2n}\sin n\theta]\},$$

$$\sigma_{r\theta}(r,\theta) = \sum_{n=0}^{\infty} r^n \{ [(n+1)(n+2)c_{1n} + (3+2n)a_{1n}]\sin(n+2)\theta$$
$$+ [(1+2n)a_{2n} + n(n+1)c_{2n}]\sin n\theta$$
$$+ (n+1)[(n+2)a_{1n}\sin(n+2)\theta + na_{2n}\sin n\theta]\ln r$$
$$+ (n+1)\theta[(n+2)a_{1n}\cos(n+2)\theta + na_{2n}\cos n\theta]\}, \text{ as } r \to 0. \tag{B4}$$

The corresponding strain field can be calculated by using the constitutive stress-strain relations (Barber, 2010):

$$\varepsilon_{rr} = \frac{\kappa+1}{8G_s}\sigma_{rr} - \frac{3-\kappa}{8G_s}\sigma_{\theta\theta}, \quad \varepsilon_{\theta\theta} = \frac{\kappa+1}{8G_s}\sigma_{\theta\theta} - \frac{3-\kappa}{8G_s}\sigma_{rr},$$
$$\varepsilon_{r\theta} = \frac{1}{2G_s}\sigma_{r\theta}, \tag{B5}$$

being $\kappa = 3-4\nu_s$ for plane strain and $\kappa = (3-\nu_s)/(1+\nu_s)$ for plane stress, respectively. After properly integrating the strain components (B5) and considering the symmetry conditions, the following displacement field in the half plane is retrieved:

$$G_s u_r(r,\theta)$$
$$= A_2 \cos\theta - A_1 \sin\theta - \frac{1}{2}\sum_{n=0}^{\infty} r^{n+1} \{ [c_{1n}(n+2) + a_{1n}]\cos(n+2)\theta$$
$$+ [c_{2n}(n+1-\kappa) + a_{2n}]\cos n\theta + [(n+2)a_{1n}\cos(n+2)\theta$$
$$+ (n+1-\kappa)a_{1n}\cos n\theta]\ln r,$$
$$- \theta[(n+2)a_{1n}\sin(n+2)\theta + (n+1-\kappa)a_{2n}\sin n\theta]\},$$

$$G_s u_\theta(r,\theta)$$
$$= B_1 r - A_1 \cos\theta - A_2 \sin\theta$$
$$+ \frac{1}{2}\sum_{n=0}^{\infty} r^{n+1} \{ [c_{1n}(n+2) + a_{1n}]\sin(n+2)\theta$$
$$+ [c_{2n}(n+1+\kappa) + a_{2n}]\sin n\theta$$
$$+ [(n+2)a_{1n}\sin(n+2)\theta + (n+1+\kappa)a_{2n}\sin n\theta]\ln r,$$
$$+ \theta[(n+2)a_{1n}\cos(n+2)\theta + (n+1+\kappa)a_{2n}\cos n\theta], \text{ as } r \to 0. \tag{B6}$$

where A_2 is a constant proportional to a rigid body motion along the vertical direction. Then, Eqs. (13) require:

$$E_b I \frac{d^4}{dr^4} u_\theta(r, \pi/2) + \sigma_{rr}(r, \pi/2) - \frac{h}{2}\frac{d}{dr}\sigma_{r\theta}(r, \pi/2) = 0,$$
$$\sigma_{r\theta}(r, \pi/2) - E_b A \frac{d^2}{dr^2}[u_r(r, \pi/2) - \frac{h}{2}\frac{d}{dr}u_\theta(r, \pi/2)] = 0, \tag{B7}$$

being $\varphi(r, \pi/2) = \frac{d}{dr} u_\theta(r, \pi/2)$. Moreover, the following condition must be imposed under the loaded section of the beam:

$$\left[E_b I \frac{d^3}{dr^3} u_\theta(r, \pi/2) \right]_{r=0} = T_0. \tag{B8}$$

The symmetry of the problem entails $u_r(0, \pm\pi/2) = 0$ and $u_\theta(r, \pi/2) = -u_\theta(r, -\pi/2)$, thus finding $A_1 = B_1 = 0$. Furthermore, according to condition (B1)$_2$, the peel stress must take a finite value under the loaded section. Such an assumption, together with the symmetry condition $\varphi(0) = 0$, implies

$$a_{10} = a_{20} = 0. \tag{B9}$$

It should be remarked that Eq. (B7) provide relations between constants of orders nth, $(n+1)$th and $(n+2)$th. Then, some of the constants can be evaluated by truncating the series expansions of the stress and displacement fields to the $(n+2)$th order, and then imposing that conditions (B7)–(B8) hold up to the order n. However, the asymptotic analysis cannot define all the coefficients. As an example, by taking the terms in the series (B2) up to the order $n = 6$, then only some of the coefficients a_{in} and c_{in} for $n = 0$–4 and $i = 1, 2$ can be assessed. In particular, the following terms can be determined from conditions (B7)–(B8) independently of the coefficients c_{in}:

$$a_{11} = -T_0 G_s h(2+\kappa)/(12\kappa\pi E_b I),$$
$$a_{21} = -T_0 G_s h/(4\kappa\pi E_b I),$$
$$a_{12} = T_0 G_s [8(\kappa-3)\kappa - (\kappa+3)(\kappa+1)G_s h(h^2/E_b I + 4/E_b A)]/$$
$$(192\kappa^2\pi E_b I),$$
$$a_{22} = -T_0 G_s [8\kappa + (\kappa+1)G_s h(h^2/E_b I + 4/E_b A)]/(48\kappa^2\pi E_b I). \tag{B10}$$

References

Abramowitz, M., Stegun, I.A., 1972. Handbook of Mathematical Functions: with Formulas, Graphs and Mathematical Tables. Dover Publications, New York.

Arutiunian, N.Kh., 1968. Contact Problem for a half-plane with elastic reinforcement. J. Appl. Math. Mech. (PMM) 32, 632–646.

Ballas, R.G., 2007. Piezoelectric Multilayer Beam Bending Actuators. Static and Dynamic Behavior and Aspects of Sensor Integration. Springer-Verlag.

Barber, J.R., 2010. Elasticity, 3rd revised edition Springer.

Barbero, E.J., 1999. Introduction to Composite Materials Design. Taylor & Francis.

Bjarnehed, H., 1993. Multiply loaded Timoshenko beam on a stressed orthotropic half-plane via a thin elastic layer. J. Appl. Mech. 60 (2), 541–547.

Boros, G., Moll, V., 2004. Irresistible Integrals. Symbolics, Analysis and Experiments in the Evaluation of Integrals. Cambridge University Press.

Cowper, G.R., 1966. The shear coefficients in Timoshenko's beam theory. ASME-J. Appl. Mech. 13 (3)-4, 335–340.

Erdogan, F., Gupta, G.D., Cook, T.S., 1973. Numerical solution of singular integral equations. "Mechanics of fracture" Vol.1: Methods of Analysis and Solutions of Crack Problems. Springer, pp. 368–425.

Erdogan, F., 1969. Approximate solutions of systems of singular integral equations. SIAM J. Appl. Math. 17 (6), 1041–1059.

Erdogan, F., Gupta, G.D., 1971. The problem of an elastic stiffener bonded to a half plane. ASME J. Appl. Mech. 38 (4), 937–941.

Erdogan, F., Ozturk, 2008. On the singularities in fracture and contact mechanics. J. Appl. Mech. 75 051111-1-12.

Essenburg, F., 1962. Shear deformation in beams on elastic foundations. J. Appl. Mech. 29 (2), 313–317.

Gevorgian, S., 2009. Ferroelectrics in microwave devices, circuits and systems. Physics, modeling, fabrication and measurements. Springer.

Gradshteyn, I.S., Ryzhik, I.M., 2007. Table of Integrals, Series, and Products. Academic Press.

Grondin, G.Y., Elwi, A.E., Cheng, J.J.R., 1999. Buckling of stiffened steel plates—a parametric study. J. Constr. Steel Res. 50, 151–175.

Guidi, V., Lanzoni, L., Mazzolari, A., Martinelli, G., Tralli, A., 2007. Design of a crystalline undulator based on patterning by tensile Si₃N₄ strips on a Si crystal. Appl. Phys. Lett. 90, 114107.

Guler, M.A., 2008. Mechanical modeling of thin films and cover plates bonded to graded substrates. J. Appl. Mech. 75 051105-1-8.

Hills, D.A., Dini, D., Magadu, A., Korsunsky, A.M., 2004. A review of asymptotic procedures in stress analysis: known solutions and their applications. J. Strain Anal. 39 (6), 553–568.

Johnson, K.L., 1985. Contact Mechanics. Cambridge University Press.

Karpenko, L.N., 1966. Approximate solution of a singular integral equation by means of Jacobi polynomials. J. Appl. Math. Mech. 30 (3), 564–569.

Lanzoni, L., Mazzolari, A., Guidi, V., Tralli, A., Martinelli, G., 2008. On the mechanical behaviour of a crystalline undulator. Int. J. Eng. Sci. 46, 917–928.

Lanzoni, L., Radi, E., 2009. Thermally induced deformations in a partially coated elastic layer. Int. J. Solids Struct 46 (6), 1402–1412.

Lanzoni, L., 2011. Analysis of stress singularities in thin coatings bonded to a semi-infinite elastic substrate. Int. J. Solids Struct. 48, 1915–1926.

Li, H., Dempsey, J.P., 1988. Unbonded contact of finite Timoshenko beam on elastic layer. J. Eng. Mech. 114, 1265–1284.

Lin, J., Liu, W.-Z., 2006. Experimental evaluation of a piezoelectric vibration absorber using a simplified fuzzy controller in a cantilever beam. J. Sound Vib. 296, 567–582.

Mahajan, R., Erdogan, F., Kilic, B., Madenci, E., 2003. Cracking of an orthotropic substrate reinforced by an orthotropic plate. Int. J. Solids Struct. 40, 6389–6415.

Moore, T.D., Jarvis, J.L., 2004. Peeling in bimaterial beams: the peeling moment and its relation to the differential rigidity. ASME J. Appl. Mech. 71, 290–292.

Morar, G.A., Popov, G.Ia., 1971. On a contact problem for a half-plane with elastic coverings. J. Appl. Math. Mech. 35 (1), 172–178.

Oehlers, D.J., Seracino, R., 2004. Design of FRP and Steel Plated RC Structures Retrofitting Beams and Slabs for Strength, Stiffness and Ductility. Elsevier Ltd.

Rice, J.R., 1988. Elastic fracture mechanics concepts for interfacial cracks. J. Appl. Mech. 55, 98–103.

Shen, Y.-L., 2010. Constrained Deformation of Materials. Devices, Heterogeneous Structures and Thermo-mechanical Modelling. Springer.

Shield, T.W., Kim, K.S., 1992. Beam theory models for thin film segments cohesively bonded to an elastic half space. Int. J. Solids Struct. 29, 1085–1103.

Sinclair, G.B., 2004. Stress singularities in classical elasticity–I: Removal, interpretation, and analysis. Appl. Mech. Rev. 57 (4), 251–297.

Suhir, E., 1988. An approximate analysis of stresses in multilayered elastic thin films. ASME J. Appl. Mech. 55, 143–148.

Suhir, E., 1989. Interfacial stresses in bimetal thermostats. ASME J. Appl. Mech. 56, 595–600.

Suhir, E., 1986. Stresses in bi-metal thermostats. ASME J. Appl. Mech. 53, 657–660.

Szegö, G., 1939. Orthogonal Polynomials. American Mathematical Society.

Takahashi, M., Shibuya, Y., 1997. Numerical analysis of interfacial stress and stress singularity between thin films and substrates. Mech. Res. Commun. 24 (6), 597–602.

Takahashi, M., Shibuya, Y., 2003. Thermoelastic analysis of interfacial stress and stress singularity between a thin film and its substrate. J. Therm. Stress. 26 (10), 963–976.

Tezzon, E., Tullini, N., Minghini, F., 2015. Static analysis of shear flexible beams and frames in adhesive contact with an isotropic elastic half-plane using a coupled FE-BIE model. Eng. Struct. 104, 32–50. doi:10.1016/j.engstruct.2015.09.017.

Timoshenko, S.P., 1925. Analysis of bi-metal thermostats. J. Opt. Soc. Am. 11, 233–255.

Tullini, N., Tralli, A., Lanzoni, L., 2012. Interfacial shear stress analysis of bar and thin film bonded to 2D elastic substrate using a coupled FE–BIE method. Finite Elements Anal. Des. 55, 42–51.

Tullini, N., Tralli, A., Baraldi, D., 2013. Buckling of Timoshenko beams in frictionless contact with an elastic half-plane. J. Eng. Mech. 139, 824–831.

Villaggio, P., 2003. Brittle detachment of a stiffener bonded to an elastic plate. J. Eng. Math. 46, 409–416.

Wang, C.M., Tan, V.B.C., Zhang, Y.Y., 2006. Timoshenko beam model for vibration analysis of multi-walled carbon nanotubes. J. Sound Vibr. 294, 1060–1072.

Williams, M.L., 1959. The stresses around a fault or crack in dissimilar media. Bull. Seism. Soc. Am. 49 (2), 199–204.

Wolf, J.P., 1988. Soil-Structure Interaction Analysis in Time Domain. Prentice-Hall, Inc.

Wu, T.X, Thompson, D.J., 1999. A double Timoshenko beam model for vertical vibration analysis of railway track at high frequencies. J. Sound Vib. 224 (2), 329–348.